

---

# THE COMPLEX-VALUED CORRELATION COEFFICIENT ACCOUNTS FOR BINAURAL DETECTION.

---

A PREPRINT

✉ **Jörg. Encke**

Department für Medizinische Physik und Akustik  
Universität Oldenburg  
26111 Oldenburg, Germany  
joerg.encke@uni-oldenburg.de

✉ **Mathias. Dietz**

Department für Medizinische Physik und Akustik  
Universität Oldenburg  
26111 Oldenburg, Germany

December 13, 2021

## ABSTRACT

Binaural hearing is one of the principal mechanisms enabling the localization of sound sources in space. In addition, binaural hearing also significantly improves the detection of signals in noise. Humans can detect interaurally anti-phasic tones in masking noise at sound levels 15 dB below the detection threshold of the equivalent in-phase tones. Intermediate thresholds result from detecting tones in noise with an interaural time difference (ITD). The dependence on ITD has so far been most accurately accounted for by models using an array of internal delays, altering, and ideally compensating for the noise ITD. The array of internal delays, or an equivalent mechanism, however, has not been found in mammals. Alternative coding principles that do not include an array of delays can also explain many aspects of sound localization but have failed to account for some of the available data on binaural detection. By employing the complex-valued correlation coefficient, we show that a minimum assumption model can explain the outcome of a wide range of binaural detection experiments. The proposed mechanism requires fewer degrees of freedom when compared to models with an array of delays while arguably improving compatibility with mammalian physiology. Intriguingly, the 2-dimensional acoustic feature space of variance normalized complex correlation coefficients is at the same time a perceptually uniform space for binaural detection.

## 1 Introduction

The auditory system has the challenging task of restoring the spatial properties of an acoustic scene based solely on the signals arriving at the two ears. A critical source of information in this process is the difference in arrival time between the signals at the two ears. The delay-line or Jeffress model [2], one of the longest-standing models of sensory-neuronal computation, suggests that an array of coincidence-detecting neurons compares neuronal signals from the two cochleae. According to this model, each neuron in the array is associated with a characteristic delay  $\tau$  compensating for a specific interaural time difference (ITD); the neuron that compensates best for the ITD would then show the strongest response. This concept corresponds to a cross-correlation and postulates a place code for ITD. The delay-line concept was supported by the success of quantitative cross-correlation-based models that were able to predict a variety of human psychoacoustic data [3–6]. Equally compelling, the predicted arrangement of axonal delay lines has been found in the nucleus laminaris of the barn owl [7], a spatial hearing specialist. In mammals, however, no such structure has been found. Instead, ITD-sensitive neurons have been associated with a rate code, where the relative firing rates of single neurons or populations of neurons encode for interaural differences [8–10].

In addition to sound localization, listening with two ears also provides a benefit in complex environments in which a target sound is masked by sounds from another location [11]. This binaural unmasking has been studied extensively using tone-in-noise detection experiments, resulting in a large body of highly reproducible data [4, 12–14].

These studies consistently found that tone-in-noise detection improves greatly when an interaural difference is introduced into either the tone or the masker. If the masker is identical in both ears, anti-phasic 500-Hz tones can be detected at a

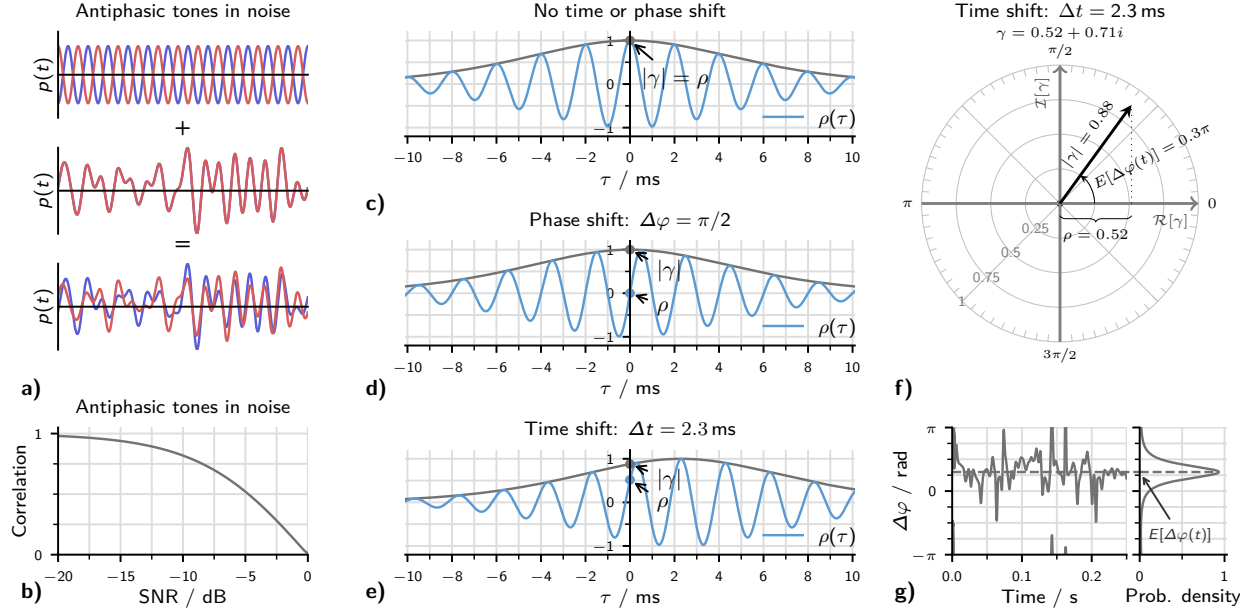


**Figure 1:** Visualization of interaural cues. **a)** Schematic visualization of the signals in a tone-in-noise experiment. In this example, anti-phasic tones (top panel) are added to the same noise token (middle panel), resulting in a partly decorrelated stimulus (bottom panel). **b)** The amount of decorrelation depends on the level of the added tone. This panel shows the correlation as a function of SNR calculated for an anti-phasic tone in noise as visualized in (a). **c)** Cross-correlation function  $\rho(\tau)$  calculated for noise after applying a 500 Hz-centered gammatone-filter with 79 Hz equivalent rectangular bandwidth (blue line). **d)** Applying a  $\pi/2$  IPD shifts the  $\rho(\tau)$  function, so that  $\rho = 0$ . The envelope of  $\rho(\tau)$ , however, remains unchanged by the IPD so that  $|\gamma|$  remains at unity. **e)** Introducing an ITD causes a shift of  $\rho(\tau)$ , including its envelope which thus influences both  $\rho$  and  $|\gamma|$ . **f)** Visualization of the different components of the complex correlation-coefficient  $\gamma$  for the same noise as in e). **g)** Instantaneous IPD  $\Delta\varphi(t)$  for the same noise as used in e) and f). The right subplot shows the corresponding probability density function [1]. The expected value of this distribution equals the argument of the stimulus coherence  $E[\Delta\varphi(t)] = \arg(\gamma) = 0.3\pi$ .

sound level 15 dB lower than for in-phase tones [12]. This benefit is purely binaural: monaural detection thresholds are unaffected by changes in tone phase, even though the waveform of the noise signal changes depending on the phase of the added tone (See Fig. 1a).

Tone-in-noise detection thresholds depend on several stimulus features, including noise correlation, noise ITD, interaural phase relation of noise and target, and noise bandwidth. Models based on the cross-correlation function account for these dependencies by detecting changes in the maximum of the cross-correlation function  $\rho(\tau)$  which are caused by the tone [3, 4]. These models benefit from the large array of differently tuned coincidence detectors which enables them to use the most informative delay element,  $\rho(\tau_{\text{best}})$ , for the respective task. Models that lack the array of delay-tuned detectors fall short in terms of both accuracy and comprehensiveness [15–17].

Adding a tone with an interaural phase difference (IPD) to a correlated masker not only reduces the correlation but also introduces fluctuations in IPD [18]. While the reduction in correlation and the fluctuation strength are closely connected, this relation does not always hold. This is illustrated by comparing two cases: (A) Two noise tokens from independent sources; (B) Two noise tokens from the same source where one token is phase-shifted by  $\pi/2$ . In both cases, the correlation between the tokens is zero. In the case of the two independent tokens, however, the IPD fluctuates randomly, whereas, by definition, (B) has a constant IPD. The amount of IPD fluctuation thus offers additional information about the underlying binaural statistics and has been proposed as an alternative metric for binaural detection [18–20].

Instead of using the IPD fluctuation directly, we propose using the complex correlation coefficient:

$$\gamma = \frac{\langle u^*(t)z(t) \rangle}{\sqrt{\langle |u(t)|^2 \rangle \langle |z(t)|^2 \rangle}}. \quad (1)$$

where  $u(t)$  and  $z(t)$  are the analytical representations of the left and right ear signals, respectively. The asterisk indicates the complex conjugate, and the angular brackets the ensemble average.

Panels f and g in Fig. 1 illustrate that  $\gamma$  contains information about both the average IPD and the amount of fluctuation around this average value. Its argument  $\arg(\gamma)$  equals the expected value of the distribution of instantaneous IPDs,

or the time averaged IPD. Its modulus  $|\gamma|$  is a measure for the consistency of left and right instantaneous phases and thus for the IPD fluctuation strength. We will refer to  $|\gamma|$  as the interaural coherence<sup>1</sup>[20]. The coherence  $|\gamma|$  can take values between 0 and 1 where 0 indicates no relation of instantaneous phases, and thus heavily fluctuating IPDs, while a value of 1 indicates a constant IPD. The word “correlation” in “complex correlation coefficient” suggests a similarity to the classic cross-correlation-function models, but it no longer relies on the internal delay parameter  $\tau$ . The encoded information is expressed only by a single complex number  $\gamma$ . The aim of this study is to test whether a computational model based on the complex cross-correlation coefficient can indeed match models based on the real-valued cross-correlation function in their predictive power to account for a large variety of binaural unmasking data.

## 2 Results

Tone-in-noise detection is usually performed as an alternative forced-choice task with one or more reference intervals containing only the reference noise and a target interval in which the tone is added to the noise. The goal of these studies is to determine the signal-to-noise ratio (SNR) at which the subject can identify the target stimulus with a predefined sensitivity.

A computational model was used to test the hypothesis that binaural tone-in-noise detection can be explained based on the complex correlation coefficient. In the model, threshold SNRs are calculated directly from the absolute difference between the complex-correlation coefficients of the masker and target stimuli. Correlation coefficients were calculated based on the spectral properties of the two input stimuli, assuming only a peripheral bandpass filter. In addition to this binaural detection path, a monaural pathway provides an SNR-based detection cue in stimuli with few or no binaural cues. A mathematical description of the model is given in the Methods.

Four stimulus parameters were necessary to define the stimuli used in this study: The IPD of the noise as a function of angular frequency  $\Delta\varphi(\omega)$ , the noise correlation  $\rho_N$ , the IPD of the target tone  $\Delta\phi$ , and the noise bandwidth  $\Delta\omega$ . For example, for an out-of phase tone in 900 Hz wide, correlated noise with 2.3 ms ITD (as used in Fig. 1e-g), the parameters would be set to  $\Delta\varphi(\omega) = \omega \times 2.3 \text{ ms}$ ,  $\rho_N = 1$ ,  $\Delta\psi = \pi$  and  $\Delta\omega = 2\pi \times 900 \text{ Hz}$ . Table 1 summarizes the stimulus parameters of all experiments that are discussed below. Three parameters define the model itself: parameters  $\sigma_{\text{bin}}$  and  $\sigma_{\text{mon}}$ , which directly determine the binaural and the monaural detection sensitivity, and a third parameter  $\hat{\rho}$ , which limits the maximal sensitivity to changes in coherence. Model parameters were optimized separately for each experiment because detection thresholds for identical stimuli were not always identical across studies. This finding is unsurprising, since most experiments were conducted with a small number of subjects. Table 1 summarizes the resulting model parameters.

### 2.1 Simulated data sets

The first data set by Pollack & Trittipoe [24] is not from a tone-in-noise experiment but directly quantified the sensitivity to changes in coherence. For the model, this sensitivity was directly calculated using Eq.7. Experimental data and model results are shown together in Fig. 2a.

In the next two experiments, the reference also consisted of noise with predefined interaural correlations. However, the target correlation was not manipulated directly but was changed by adding a tone to the partly correlated noise. Robinson & Jeffress [25] collected results for both in-phase and anti-phasic tones (See Fig. 2b). The experiment with anti-phasic tones was repeated by Bernstein & Trahiotis [26], who also collected data at different noise bandwidths (See Fig. 2c). The change in coherence that arises from adding a tone at a given SNR depends on the initial noise correlation  $\rho_N$  and on the difference between the tone IPD and the noise IPD [27]. The coherence change is greatest when the two IPDs are out of phase, while there is no influence when the IPDs are the same. In Fig. 2b, this is reflected in the large difference between the threshold SNRs of the in-phase and anti-phasic conditions when  $\rho_N = -1$  and  $\rho_N = 1$ . The improvement in threshold SNR with increasing bandwidth, as seen in Fig. 2c, can be explained solely by the filter property of the auditory periphery. Only noise energy that falls within the peripheral filter interacts with the tone and thus determines the coherence. This peripheral filtering improves the SNR and thus also the nominal threshold SNR. For large stimulus bandwidths far exceeding the peripheral bandwidth, this improvement equals 3 dB/octave.

<sup>1</sup>There are several definitions of coherence. Our use of coherence as  $|\gamma|$  is a typical time-domain definition, as it is commonly used in fields of physics that deal with waves, such as optics [21]. In general signal processing, the coherence function is instead defined in the frequency domain and calculated as the normalized absolute value of the cross spectral power density (CSPD) [22]. The two definitions are strongly related, as the time-domain coherence can also be defined by using a Fourier-transform of the CSPD (see methods for details). In binaural research, a third definition exists, where interaural coherence is sometimes used to refer to the maximum of the real-valued cross-correlation function [23]. This definition, however, is unique to the sub-domain and deviates from the other two.

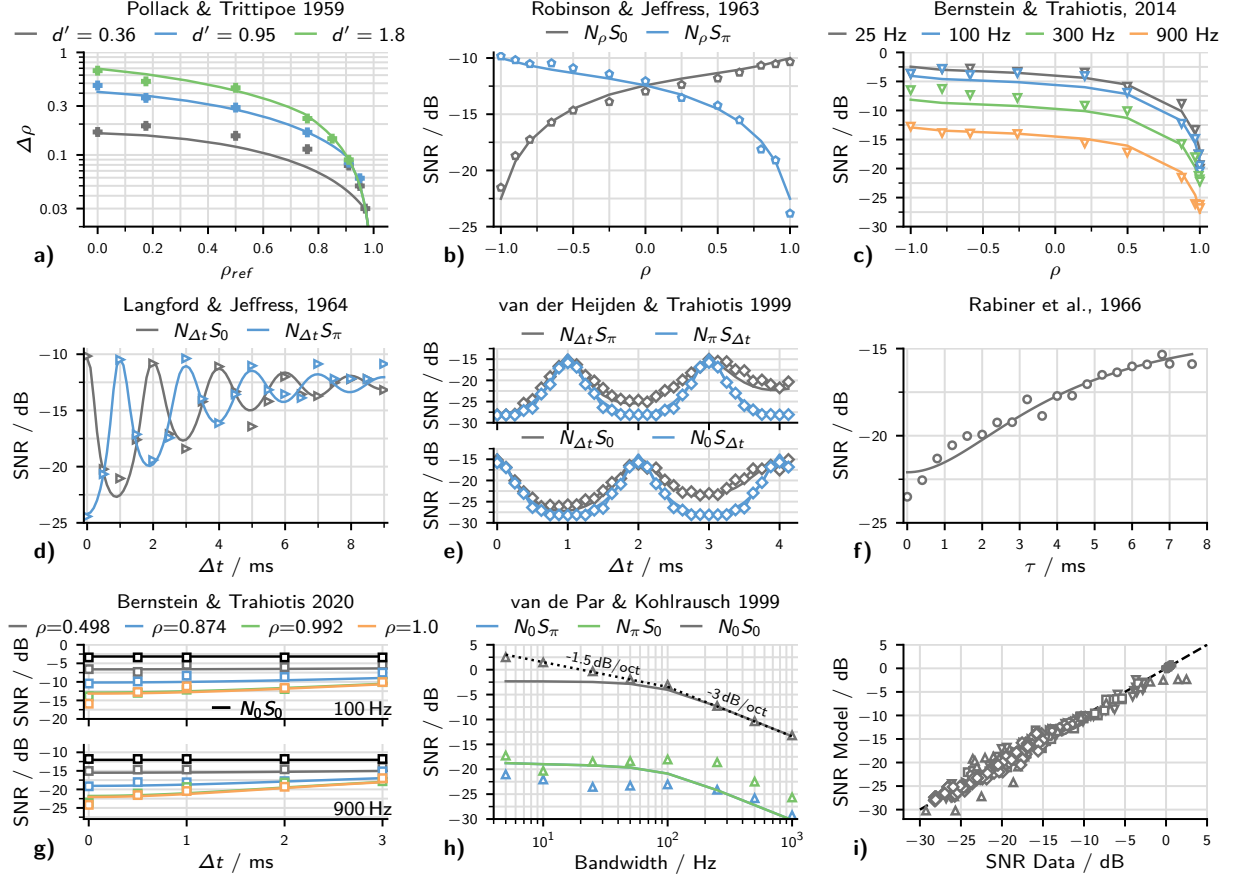


**Figure 2:** Experimental data and model results for all experiments. In all cases, symbols indicate the experimental data as digitized from the respective study. Simulated thresholds are shown as lines in matching color. **a)** Incoherence detection thresholds. The reference noise-correlation serves as abscissa and the required change in correlation as ordinate. The different colors indicate different sensitivity indices, i.e. different threshold definitions. **b-h)** Threshold SNRs for seven different studies with the threshold defined as in the respective study. Colors differentiate between conditions. **b)** Dependence on noise correlation. Colors differentiate between the use of in-phase ( $N_\rho S_0$ ) or anti-phasic ( $N_\rho S_\pi$ ) tones. **c)** The same experiment as in b) for anti-phasic tones only. Colors mark different stimulus bandwidths. **d)** Dependence on noise-ITD. Colors indicate the use of an in-phase (grey) or anti-phasic (blue) target tone. **e)** The same experiment as in d) with higher ITD resolution (grey data). Additional conditions depict thresholds when the ITD was applied to the tone instead of the noise (blue). **f)** Similar to d) but instead of a regular ITD, the ITD is only applied to the envelope of the noise. **g)** Similar to d) but the ITD is applied to the whole stimulus (noise and tone). Colors indicate different noise correlations while the  $N_0 S_0$  condition is shown in black. Data for a 100 Hz masker bandwidth is shown on the top and for 900 Hz on the bottom. Results for the  $\rho = 0.992$  condition are partly concealed by those of the  $\rho = 1.0$  condition. **h)** Dependence on stimulus bandwidth. Colors mark the interaural configuration, including one without binaural cues (grey). Model results for the  $N_0 S_\pi$  condition are concealed by those for the  $N_\pi S_0$  condition. **i)** Summarizing scatter plot of all 329 simulated threshold SNRs plotted against their experimental counterpart. The dashed diagonal indicates points of equality. Symbols correspond to the respective symbols from panels b-h.

Instead of directly changing the masking noise correlation, the next set of studies by Langford & Jeffress [13] and van der Heijden & Trahiotis [4] applied an ITD to the noise before adding the target tone (Fig. 2d and e). The added ITD results in both a reduction in coherence  $|\gamma|$  and a shift in the noise IPD (See Fig. 1e-f for an example). The change in noise IPD results in periodic oscillations of the threshold SNR, as the effectiveness of the added phasic or anti-phasic tone changes with noise IPD. The periodic oscillation is superimposed by an overall increase in threshold SNR with ITD. Rabiner et al. [14] conducted a slightly different but related experiment: Instead of applying the ITD to the whole noise, it was applied only to the envelope of the masking noise which keeps the noise-IPD fixed at zero (Fig. 2f). Doing this removes the oscillations in the threshold SNR while resulting in the same increase in threshold SNR as when using the regular ITD.

Yet another stimulus variation was introduced by Bernstein & Trahiotis [28] who added anti-phasic tones to noises of different interaural correlations and applied the ITD to the whole signal. This modification keeps the phase relation

**Table 1:** Aggregation of stimulus and model parameters used to simulate experiments from eight different studies. The last column states the resulting coefficient of determination  $R^2$ , which can be interpreted as the proportion of the variance in the data set that is explained by the model. The last row lists a single set of parameters that was optimized to minimize  $R^2$  for all experiments.

Study	$\Delta\varphi(\omega)$	Stimulus parameter			Model parameter			$R^2$	
		$\rho_N$	$\Delta\psi$	$\Delta\omega/2\pi$	$\hat{\rho}$	$\sigma_{\text{bin}}$	$\sigma_{\text{mon}}$		
Pollack & Trittipoe 1959	0	$\rho + \Delta\rho$	/	1 kHz	0.92	0.42	/	0.97	
Robinson & Jeffress 1963		-1 to 1	$0, \pi$	0.9 kHz	0.92	0.31	0.76	0.98	
Bernstein & Trahiotis 2014		-1 to 1	$\pi$	25 Hz to 0.9 kHz	0.97	0.54	0.76	0.97	
Langford & Jeffress 1964		$\omega\Delta t$	1	0, $\pi$	0.9 kHz	0.95	0.33	0.70	0.96
van der Heijden & Trahiotis 1999		$\omega\Delta t$	1	0, $\pi$	0.9 kHz	0.90	0.19	0.61	0.95
Rabiner et al. 1966		$(\omega - \omega_0)\Delta t$	1	$\pi$	1.1 kHz	0.85	0.24	0.71	0.95
Bernstein & Trahiotis 2020		$\omega\Delta t$	0.498 to 1	$\omega_0\Delta t + \pi$	0.1 kHz, 0.9 kHz	0.89	0.52	0.93	0.96
van de Par & Kohlrausch 1999		$0, \pi$	1	0, $\pi$	5 Hz to 1 kHz	0.97	0.38	0.76	0.91
Individual parameters optimized for each experiment:								0.98	
One parameter set optimized for all experiments:						0.96	0.40	0.74	0.93

between noise IPD and tone IPD fixed at  $\pi$  so that the ITD only influences the stimulus coherence (Fig. 2g). As in the study by Rabiner et al. [14], this results in an increase in the threshold SNR without oscillations. The increase is less pronounced at low noise correlations because the effect of the ITD on coherence diminishes with decreasing noise correlation.

As described above, the model accounts for the bandwidth dependence of detection thresholds because of its bandpass filter. Figure 2h shows experimental results from van de Par & Kohlrausch [29] as well as simulated threshold SNRs for a large range of bandwidths from 5 Hz to 1 kHz in two configurations with binaural cues and one configuration with monaural cues only. At very low bandwidths, the filter does not significantly affect the noise energy, so the threshold SNR remains constant. At large bandwidths, the predicted threshold SNR improves by 3 dB per octave.

With parameters that were optimized individually for each experiment, the model could account for 91% to 98% of the respective variance (See Tbl. 1). For all data sets together, keeping the individual parameters, the model accounted for 98% of the total variance. Figure 2i visualizes this high correlation between modeled and experimental thresholds by plotting one against the other. A single set of parameters, optimized to reduce the variance across all data sets, still accounted for 93% of the total variance, despite the deviations in experimental threshold for identical stimulus parameters mentioned above.

### 3 Discussion

The complex-valued correlation coefficient model proposed here was able to account for nearly all aspects of the psychophysical data sets examined in this study. The modeled binaural sensitivity is directly proportional to the difference in the z-transformed complex correlation coefficient  $\gamma$  between target and reference. The bandpass filter is the only pre-processing stage necessary to account for these data sets. The following discussion will thus focus on these two components of the model while also considering possible neuronal substrates for the proposed mechanism.

#### 3.1 Implications of the complex correlation coefficient

In the first three experiments (Fig. 2a to c), no phase or time-shifts were added to the signal. Consequently, the imaginary part of  $\gamma$  was always 0 so that  $\gamma$  equaled the real-valued correlation coefficient ( $\gamma = \rho$ ). This means that the model would show identical results if it were based solely on  $\rho$ . The comprehensiveness and accuracy of  $\rho$ -based models for this kind of stimuli has been demonstrated previously [3].

The experiments shown in Fig. 2d-i, included ITDs or IPDs, so that  $\gamma$  was generally not real-valued. In these cases, models based on real-valued correlation alone need to include larger parts of the cross-correlation function  $\rho(\tau)$  [3, 4]. Alternatively, as shown in this study, this kind of data can be explained entirely by the complex correlation coefficient. To better understand the underlying mechanism, Figure 3a visualizes the z-transformed coefficients for threshold SNRs for the data of van der Heijden & Trahiotis, [4]. The illustrated complex space can be interpreted as a binaural feature space, where the distance between reference and target is directly proportional to the binaural sensitivity  $d_{\text{bin}}$ . It is apparent that this distance is determined by both the coherence, reflected in the length of the vector, and the mean IPD, reflected in its angle. The relative contributions of length and angle depend on the specific stimulus condition. For conditions where the difference between mean IPD of the noise and the tone equals 0 or  $\pi$ , the added tone cannot

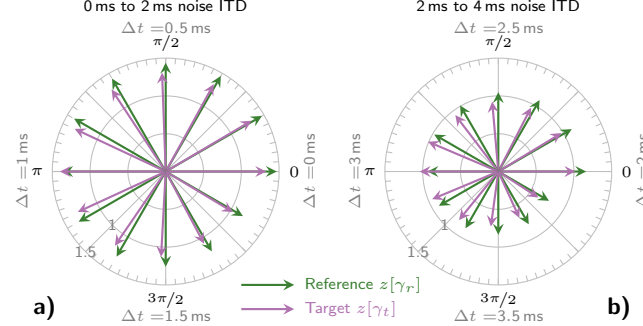


**Figure 3:** Vector visualization of the z-transformed correlation coefficients for selected stimuli of the  $\mathbf{N}_{\Delta t} \mathbf{S}_{\pi}$ ) condition of van der Heijden & Trahiotis [4] (also see Fig. 2. Results for reference stimuli are shown in green while target stimuli are shown in purple. The length of each vector represents the z-transformed coherence of the respective stimulus, while the angle represents the mean IPD. Target stimuli, shown in purple, contain both tone and noise at the experimental threshold SNR. Noise-ITDs in the range of 0 ms-2 ms are shown in panel a) and 2 ms-4 ms in panel b). Changes in  $\Delta t$  are directly reflected in the average noise-IPD, which determines the polar angle of the reference, so polar-labels state both the angle and the respective noise-ITD. The distance between the tips of the reference and target vectors is directly proportional to the strength of the binaural cue.

influence the mean IPD of the resulting signal. In these cases, binaural detection was based solely on a change in coherence. If the difference is  $\pi$ , the coherence change caused by the target is large, so the binaural cue is generally large as well. When the difference is 0, detection relied mostly on monaural cues, as visible in Fig. 3a: the vectors of reference and target are nearly equal at  $\Delta t = 1$  ms. In this situation, the availability of binaural cues increases with decreasing noise coherence, as the added tone can then increase the coherence of the target relative to the reference (see  $\Delta t = 3$  ms in Fig. 3b). The decrease in coherence with ITD is visible in the decreasing length of the reference vectors.

Of the data simulated in the present study, only that of van der Heijden & Trahiotis [4] and Langford & Jeffress [13] include stimuli with mean IPD differences between noise and tone other than 0 or  $\pi$ . Only these intermediate differences cause a change in both coherence and angle of the target stimulus (Fig.3). In these intermediate cases, it is particularly advantageous to use the complex plane of the z-transformed correlation coefficient  $z[\gamma]$  as a two-dimensional acoustic stimulus feature space. A key finding of the present study is that the acoustic feature space can be used directly as a perceptual feature space so that the distance between two stimuli in this space is proportional to the binaural sensitivity index  $d'_{\text{bin}}$ . The complex plane of  $z[\gamma]$  can thus be interpreted as a perceptually uniform space like, for example, the CIELAB color space that is commonly used to represent color difference sensitivity [30].

If  $z[\gamma]$  is interpreted as a perceptually uniform space, it should be possible to use the same space to explain related phenomena, such as ITD discrimination. For tones, ITDs are equivalent to IPDs. Since IPDs are reflected in the argument of  $\gamma$ , IPD discrimination sensitivity can be directly derived from Eq. 7:

$$\Delta\sigma_{\text{thr}} = 2 \arcsin \left( \frac{d'_{\text{bin}} \sigma_{\text{bin}}}{2 \operatorname{arctanh}(\hat{\rho})} \right). \quad (2)$$

Using the set of parameters summarized in Tbl 1. with  $d'_{\text{bin}} = 1$  resulted in IPD thresholds equivalent to ITDs in the range of  $41 \mu\text{s}$  to  $117 \mu\text{s}$  (Median  $60 \mu\text{s}$ ); this is within the range of experimentally obtained thresholds at 500 Hz. For discrimination around zero ITD, experimental thresholds are on average a little lower [31], but for discrimination around  $\pi$  thresholds are above the model median [32].

### 3.2 Effect of the peripheral filter bandwidth

In cases where the noise bandwidth is considerably larger than the peripheral filter bandwidth, the coherence function  $|\gamma(\tau)|$  is fully determined by the power spectrum of the peripheral filter (See Eq. 3 and 4). By substituting  $\tau$  with the ITD, the same function can be used to describe the ITD dependence of  $|\gamma|$ . In the absence of a delay line, the decline of the binaural benefit with masker ITD is therefore a direct cause of the bandwidth after filtering. Langford & Jeffress were the first to describe this relation, and coarsely estimated that a 100-Hz filter bandwidth explains the ITD dependence of their data (see Fig. 2d) [13]. With a more quantitative analysis, and assuming a triangular filter, Rabiner et al. [14] found that their data (see Fig.2f) was best accounted for by a filter with 85 Hz equivalent rectangular bandwidth (ERB). This value is close to the 79 Hz ERB of the 4<sup>th</sup> order gammatone filter that was used in the present study (see Methods). The ERB was fixed at 79 Hz in order to reduce the number of free model parameters. This bandwidth is a typical estimation for the bandwidth of the monaural periphery [33] and has also been employed in other

binaural detection models [3, 34]. The same filter bandwidth is also responsible for the change in threshold SNR with stimulus bandwidth, as seen in Fig. 2c, where the point at which the simulated threshold SNR starts to decrease is determined primarily by the bandwidth.

### 3.3 Limitations of the model implementation

While the proposed model was able to account for nearly all characteristics of the data sets shown in Fig. 2, some limitations do remain.

The experiment shown in Fig. 2h revealed differences between the threshold SNRs for in-phase tones in anti-phasic noise ( $\mathbf{N}_\pi \mathbf{S}_0$ ) and anti-phasic tones in in-phase noise ( $\mathbf{N}_0 \mathbf{S}_\pi$ ): thresholds in the  $(\mathbf{N}_\pi \mathbf{S}_0)$  condition were about 4 dB higher than for  $\mathbf{N}_0 \mathbf{S}_\pi$ . The same trend can be seen in the data shown in Fig. 2b and is consistent across other studies [12, 25]. For our model, the two conditions differ only in their mean IPD (that is, in the argument of the correlation coefficient  $\arg(\gamma)$ ), which is zero for the  $\mathbf{N}_0 \mathbf{S}_\pi$  condition and  $\pi$  for  $\mathbf{N}_\pi \mathbf{S}_0$ . By using  $\gamma$  to predict thresholds directly, the model assumes that the sensitivity to IPDs does not depend on the mean IPD, so predictions for the two conditions are the same. The mean IPD-dependent difference in the experimental thresholds also reflects the previously mentioned difference in sensitivity to changes in IPD, which is lower around  $\pi$  than around 0 [32]. Both changes in sensitivity could be caused by differences in neuronal coding precision. The responses of IPD-sensitive neurons in the auditory brainstem and midbrain usually show their strongest change around IPDs of zero; this has been suggested to facilitate the accurate encoding of IPDs in this region [8, 35]. The shape of the IPD rate functions of these neurons has also been shown to increase IPD sensitivity near zero IPD [36].

Other limitations in explaining experimental data arose from the decision to minimize the model's complexity. In the  $\mathbf{N}_0 \mathbf{S}_0$  condition shown in Fig. 2h, the model deviates significantly from the data. This deviation results from the sample-to-sample variability of the noise energy, which changes with stimulus bandwidth [29]. This effect cannot be accounted for by the current model implementation, which is based on infinitely long signals. However, a numeric implementation based on finite signal waveforms should account for this phenomenon. The current model also neglects peripheral processing apart from bandpass filtering. Without this pre-processing, the model cannot account for effects that are associated with the periphery [37–39]. Extending the current model with a more detailed periphery should help account for these data sets.

Another limitation of the current implementation is its focus on a single frequency channel centered at 500 Hz. With different parametrization, the model can be reasonably expected to account for experiments at different frequencies. Other experiments, however, such as those employing spectrally complex maskers or maskers constructed from two noise sources with different ITDs, might require a multi-channel implementation of the model. The success of this kind of model extension has recently been demonstrated [40].

### 3.4 Neuronal substrate

No additional transformation was necessary in order to use the stimulus space  $z[\gamma]$  as the perceptual space. This suggests that information virtually equivalent to the complex correlation coefficient is encoded neuronally. The question is, what is the underlying neuronal mechanism? In order to encode information equivalent to the complex correlation coefficient, neurons would have to encode either the real and imaginary parts of the coefficient, or its modulus (coherence) and argument (time-average IPD).

One possibility is that there are two differently tuned coincidence-detecting neurons or neuron populations, one responding maximally to an ITD equivalent to an IPD of  $+\pi/4$ , the other to an IPD of  $-\pi/4$ . The  $\pi/2$  difference between the two corresponds to the phase difference between the real and imaginary parts of  $\gamma$ . This kind of two-channel code has indeed been proposed as an alternative to the systematic arrangement of delay-lines, which mammals seem to lack [8]. While the original idea of the two-channel code was limited to encoding IPD and interaural coherence in isolation [20], it can also encode the complex correlation coefficient. This two channel idea is supported by the high prevalence of neurons with a maximum response at IPDs near  $\pi/4$  [8, 41]. The direct relation between correlation function and neuron responses is of course idealized, as the shape of the IPD-rate function and the inter-channel phase shift vary considerably between neurons. Any deviations from the optimal shape such as the  $\pi/2$  phase shift or the sinusoidal shape, would only skew the encoded complex plane; this could explain differences in the precision with which certain IPDs are encoded and thus the above-mentioned difference in binaural detection thresholds between in-phase and anti-phasic noise maskers [42].

The second method for encoding information akin to the complex correlation coefficient is to directly encode the time-averaged IPD and the coherence. The ability of the auditory system to encode for the former is well established [10]. To encode information equivalent to coherence, the auditory system could rely on the amount with which the

IPD fluctuates around its mean. This IPD-fluctuation code would have the benefit of only requiring information about a single quantity – the IPD – but would also require neurons fast enough to follow the instantaneous changes in IPD caused by a reduction in coherence. Neurons that do just this have been described: IPD-sensitive neurons are able to encode the fast fluctuations, by means of fast changes in their response rate [43–45]. Both proposed methods for encoding the complex correlation coefficient are therefore physiologically plausible.

### 3.5 Summary

Our goal was to test whether the complex-valued correlation coefficient can explain binaural tone-in-noise detection. Using a computational model, we were able to demonstrate that this metric is indeed able to accurately account for many central aspects of tone-in-noise detection. By relying on the complex correlation coefficient  $\gamma$  instead of the real-valued cross-correlation function  $\rho(\tau)$ , the new approach represents a significant simplification over previous modeling approaches while at the same time improving compatibility with mammalian physiology.

## Methods

The following sections introduce the underlying mathematics that were used for the model implementation. A Python implementation of the model as well as the scripts for deriving and plotting predictions for all experiments are openly available [46].

### Deriving the complex correlation-coefficient for tone-in-noise detection experiments

Throughout this study, the complex correlation coefficient was calculated from the cross-spectral power density (CSPD)  $S(\omega)$  of the signals. Following the Wiener-Khinchine theorem, the cross-correlation function of two signals is equivalent to the inverse Fourier-transform of their CSPD [47]. Consequently, the normalized complex correlation coefficient can be calculated as:

$$\gamma = \frac{\int_{-\infty}^{\infty} S(\omega) d\omega}{\sqrt{\int_{-\infty}^{\infty} |S_{uu}(\omega)| d\omega \int_{-\infty}^{\infty} |S_{zz}(\omega)| d\omega}}. \quad (3)$$

Where  $S_{uu}(\omega)$  and  $S_{zz}(\omega)$  are the power spectral densities of  $u(t)$  and  $z(t)$ . This CSPD-based approach has the benefit of directly resulting in the expected value of  $\gamma$  as opposed to a waveform-based implementation where the coherence would have to be estimated as the mean of several instances of the signal waveform.

Given the analytical representations of the left and right signals  $u(t)$  and  $z(t)$ , the effective CSPD  $S(\omega)$  was composed of two parts: The CSPD  $S_{uz}$  of  $u(t), z(t)$  and of a transfer function  $H(\omega)$  used to account for the bandpass properties of the auditory periphery:

$$S(\omega) = S_{uz}|H(\omega)|^2. \quad (4)$$

The CSPD  $S_{uz}$  is directly determined by the stimulus used in the respective experiment and can be formalized as:

$$S_{uz}(\omega) = \begin{cases} \frac{\rho_N}{\Delta\omega} e^{i\Delta\varphi(\omega)}, & \omega_0 - \frac{\Delta\omega}{2} \leq \omega \leq \omega_0 + \frac{\Delta\omega}{2} \\ \frac{\rho_N}{\Delta\omega} e^{i\Delta\varphi(\omega_0)} + \text{SNR} e^{i\Delta\psi}, & \omega = \omega_0 \\ 0, & \text{otherwise} \end{cases} \quad (5)$$

where  $\Delta\omega$  is the bandwidth of a rectangular noise band centered around  $\omega_0$  which, in all cases was set to  $\omega_0/2\pi = 500$  Hz.  $\Delta\varphi(\omega)$  is the IPD spectrum of the noise while  $\Delta\psi$  is the IPD of the tone. Both were set according to the conditions used in the respective experiment as summarized in Table 1. For tone-in-noise detection experiments,  $\gamma$  is independent of the absolute level and only depends on the SNR. Consequently, the noise energy was set to one, so that the energy of the tone equals the SNR. Some experiments also made use of noises with different interaural correlations  $\rho_N$ . The CSPD only contains interaurally coherent energy so that, in these cases, the CSPD of the noise is scaled by  $\rho_N$ . Assuming the power spectrum of a gammatone filters to account for the bandpass characteristics of the auditory periphery,  $|H(\omega)|^2$  was approximated by:

$$|H(\omega)|^2 = \left[ 1 + \frac{(\omega - \omega_0)^2}{4\pi^2 b} \right]^{-n}, b = \frac{\text{ERB}(n-1)!^2}{\pi(2n-2)! 2^{(2-2n)}} \quad (6)$$

where  $n$  is the order of the filter and ERB its equivalent rectangular bandwidth [48]. In this study, the filter was centered at 500 Hz with the filter order set to  $n = 4$  and the ERB to 78.7 Hz.

### Modeling the detection performance

A signal-detection model with two branches, one binaural and one monaural, was used to derive tone-in-noise detection thresholds. The first branch calculates the binaural sensitivity index  $d'_{\text{bin}}$  based on the difference of the complex correlation coefficients  $\gamma_r$  of a reference signal and of a target signal  $\gamma_t$ :

$$d'_{\text{bin}} = \frac{|z[\hat{\rho} \gamma_r] - z[\hat{\rho} \gamma_t]|}{\sigma_{\text{bin}}}. \quad (7)$$

Here,  $z[\bullet]$  symbolizes the Fisher's z-transform applied to the modulus of the input while leaving the argument unchanged. This transform normalizes the sampling distribution of the coherence[49]. Direct use of this transformation would result in infinite sensitivity to changes from a coherence of one so that the model parameter  $\hat{\rho}$  was introduced. Functionally, this is equivalent to adding uncorrelated noise to the two input signals to account for processing errors on the auditory pathway [50]. The sensitivity of the binaural path is adjusted by the model parameter  $\sigma_{\text{bin}}$ .

The monaural branch offers sensitivity to increases in stimulus energy between reference and target. As the power of the noise is held constant, this increase is directly proportional to the SNR so that the monaural sensitivity index  $d'_{\text{mon}}$  is calculated as:

$$d'_{\text{mon}} = \frac{\text{SNR}_{\text{eff}}}{\sigma_{\text{mon}}}, \quad (8)$$

where  $\text{SNR}_{\text{eff}}$  is the effective SNR after peripheral bandpass filtering and  $\sigma_{\text{mon}}$  is used to adjust the sensitivity of the monaural pathway.

Assuming a linear independent combination of the monaural and the binaural information, the monaural and binaural sensitivity indices are then combined to the overall sensitivity index:

$$d' = \sqrt{d'^2_{\text{bin}} + d'^2_{\text{mon}}}. \quad (9)$$

All signals that were used in this study are defined by the noise-IPD-spectrum  $\Delta\varphi(\omega)$ , the tone-IPD  $\Delta\psi$ , the noise-correlation  $\rho_N$  and the noise bandwidth  $\Delta\omega$ . With these parameters defined,  $d'_{\text{mon}}$  and  $d'_{\text{bin}}$  and thus  $d'$  only depend on the SNR. Finding the SNR that results in the  $d'$  value corresponding to the experimentally defined threshold was solved by using a numeric optimization algorithm.

## Acknowledgments

This work was supported by the European Research Council (ERC) under the European Union's Horizon 2020 Research and Innovation Programme grant agreement No. 716800 (ERC Starting Grant to M.D.)

## References

- [1] D Just, R Bamler, Phase statistics of interferograms with applications to synthetic aperture radar. *Appl. Opt.* **33**, 4361 (1994). doi:10.1364/ao.33.004361.
- [2] LA Jeffress, A place theory of sound localization. *J. Comp. Physiol. Psychol.* **41**, 35–39 (1948). doi:10.1037/h0061495.
- [3] LR Bernstein, C Trahiotis, An interaural-correlation-based approach that accounts for a wide variety of binaural detection data. *The J. Acoust. Soc. Am.* **141**, 1150–1160 (2017). doi:10.1121/1.4976098.
- [4] M van der Heijden, C Trahiotis, Binaural detection as a function of interaural correlation and bandwidth of masking noise: Implications for estimates of spectral resolution. *The J. Acoust. Soc. Am.* **103**, 1609–1614 (1998). doi:10.1121/1.421295.
- [5] HS Colburn, Theory of binaural interaction based on auditory-nerve data. i. general strategy and preliminary results on interaural discrimination. *The J. Acoust. Soc. Am.* **54**, 1458–1470 (1973). doi:10.1121/1.1914445.
- [6] HS Colburn, Theory of binaural interaction based on auditory-nerve data. ii. detection of tones in noise. *The J. Acoust. Soc. Am.* **61**, 525–533 (1977). doi:10.1121/1.381294.
- [7] CE Carr, M Konishi, Axonal delay lines for time measurement in the owl's brainstem. *Proc. Natl. Acad. Sci.* **85**, 8311–8315 (1988).
- [8] D McAlpine, D Jiang, AR Palmer, A neural code for low-frequency sound localization in mammals. *Nat. Neurosci.* **4**, 396–401 (2001). doi:10.1038/86049.
- [9] GC Stecker, IA Harrington, JC Middlebrooks, Location coding by opponent neural populations in the auditory cortex. *PLoS Biol.* **3**, e78 (2005). doi:10.1371/journal.pbio.0030078.
- [10] B Grothe, M Pecka, D McAlpine, Mechanisms of sound localization in mammals. *Physiol. Rev.* **90**, 983–1012 (2010). doi:10.1152/physrev.00026.2009.
- [11] EC Cherry, Some experiments on the recognition of speech, with one and with two ears. *The J. Acoust. Soc. Am.* **25**, 975–979 (1953). doi:10.1121/1.1907229.
- [12] IJ Hirsh, The influence of interaural phase on interaural summation and inhibition. *The J. Acoust. Soc. Am.* **20**, 536–544 (1948). doi:10.1121/1.1906407.
- [13] TL Langford, LA Jeffress, Effect of noise crosscorrelation on binaural signal detection. *The J. Acoust. Soc. Am.* **36**, 1455–1458 (1964). doi:10.1121/1.1919224.
- [14] LR Rabiner, CL Laurence, NI Durlach, Further results on binaural unmasking and the ec model. *The J. Acoust. Soc. Am.* **40**, 62–70 (1966). doi:10.1121/1.1910065.

- [15] M Dietz, SD Ewert, V Hohmann, B Kollmeier, Coding of temporally fluctuating interaural timing disparities in a binaural processing model based on phase differences. *Brain Res.* **1220**, 234–245 (2008). doi:10.1016/j.brainres.2007.09.026.
- [16] M Takanen, O Santala, V Pulkki, Visualization of functional count-comparison-based binaural auditory model output. *Hear. Res.* **309**, 147–163 (2014). doi:10.1016/j.heares.2013.10.004.
- [17] T Marquardt, D McAlpine, Masking with interaurally “double-delayed” stimuli: The range of internal delays in the human brain. *The J. Acoust. Soc. Am.* **126**, EL177–EL182 (2009). doi:10.1121/1.3253689.
- [18] E Zwicker, G Henning, The four factors leading to binaural masking-level differences. *Hear. Res.* **19**, 29–47 (1985). doi:10.1016/0378-5955(85)90096-6.
- [19] MJ Goupell, WM Hartmann, Interaural fluctuations and the detection of interaural incoherence: Bandwidth effects. *The J. Acoust. Soc. Am.* **119**, 3971–3986 (2006). doi:10.1121/1.2200147.
- [20] T Marquardt, D McAlpine, *A  $\pi$ -Limit for Coding ITDs: Implications for Binaural Models*, eds. B Kollmeier, et al. (Springer, Berlin, Heidelberg), pp. 407–416 (2007).
- [21] B Saleh, *Fundamentals of photonics*. (Wiley-Interscience, Hoboken, N.J), (2007).
- [22] K Shin, *Fundamentals of signal processing for sound and vibration engineers*. (John Wiley & Sons, Chichester, England Hoboken, NJ), (2008).
- [23] J Blauert, *Spatial hearing : the psychophysics of human sound localization*. (MIT Press, Cambridge, Mass), (1983).
- [24] I Pollack, WJ Trittipoe, Binaural listening and interaural noise cross correlation. *The J. Acoust. Soc. Am.* **31**, 1250–1252 (1959). doi:10.1121/1.1907852.
- [25] DE Robinson, LA Jeffress, Effect of varying the interaural noise correlation on the detectability of tonal signals. *The J. Acoust. Soc. Am.* **35**, 1947–1952 (1963). doi:10.1121/1.1918864.
- [26] LR Bernstein, C Trahiotis, Accounting for binaural detection as a function of masker interaural correlation: Effects of center frequency and bandwidth. *The J. Acoust. Soc. Am.* **136**, 3211–3220 (2014). doi:10.1121/1.4900830.
- [27] RH Domnitz, HS Colburn, Analysis of binaural detection models for dependence on interaural target parameters. *The J. Acoust. Soc. Am.* **59**, 598–601 (1976). doi:10.1121/1.380904.
- [28] LR Bernstein, C Trahiotis, Binaural detection as a joint function of masker bandwidth, masker interaural correlation, and interaural time delay: Empirical data and modeling. *The J. Acoust. Soc. Am.* **148**, 3481–3488 (2020). doi:10.1121/10.0002869.
- [29] S van de Par, A Kohlrausch, Dependence of binaural masking level differences on center frequency, masker bandwidth, and interaural parameters. *The J. Acoust. Soc. Am.* **106**, 1940–1947 (1999). doi:10.1121/1.427942.
- [30] International Organization for Standardization, Colorimetry – Part 4: CIE 1976 L\*a\*b\* colour space, (International Organization for Standardization, Geneva, CH), Standard (2019).
- [31] A Brughera, L Dunai, WM Hartmann, Human interaural time difference thresholds for sine tones: The high-frequency limit. *J. Acoust. Soc. Am.* **133**, 2839 (2013). doi:10.1121/1.4795778.
- [32] WA Yost, Discriminations of interaural phase differences. *J. Acoust. Soc. Am.* **55**, 1299 (1974). doi:10.1121/1.1914701.
- [33] BR Glasberg, BC Moore, Derivation of auditory filter shapes from notched-noise data. *Hear. Res.* **47**, 103–138 (1990). doi:10.1016/0378-5955(90)90170-t.
- [34] J Breebaart, S van de Par, A Kohlrausch, Binaural processing model based on contralateral inhibition. i. model structure. *The J. Acoust. Soc. Am.* **110**, 1074–1088 (2001). doi:10.1121/1.1383297.
- [35] A Brand, O Behrend, T Marquardt, D McAlpine, B Grothe, Precise inhibition is essential for microsecond interaural time difference coding. *Nature* **417**, 543–7 (2002). doi:10.1038/417543a.
- [36] TM Shackleton, BC Skottun, RH Arnott, AR Palmer, Interaural time difference discrimination thresholds for single neurons in the inferior colliculus of guinea pigs. *The J. Neurosci.* **23**, 716–724 (2003). doi:10.1523/jneurosci.23-02-00716.2003.
- [37] DA Eddins, LE Barber, The influence of stimulus envelope and fine structure on the binaural masking level difference. *The J. Acoust. Soc. Am.* **103**, 2578–2589 (1998). doi:10.1121/1.423112.
- [38] JW Hall, JH Grose, WM Hartmann, The masking-level difference in low-noise noise. *The J. Acoust. Soc. Am.* **103**, 2573–2577 (1998). doi:10.1121/1.422778.
- [39] LR Bernstein, S van de Par, C Trahiotis, The normalized interaural correlation: Accounting for nos $\pi$  thresholds obtained with gaussian and “low-noise” masking noise. *The J. Acoust. Soc. Am.* **106**, 870–876 (1999). doi:10.1121/1.428051.
- [40] B Eurich, J Encke, SD Ewert, M Dietz, Interaural coherence across frequency channels accounts for binaural detection in complex maskers (arXiv 2110.02695) (2021).
- [41] PX Joris, BV de Sande, DH Louage, M van der Heijden, Binaural and cochlear disparities. *Proc. Natl. Acad. Sci.* **103**, 12917–12922 (2006). doi:10.1073/pnas.0601396103.
- [42] J Encke, Ph.D. thesis (Technical University of Munich) (2019).
- [43] PX Joris, B van de Sande, A Recio-Spinoso, M van der Heijden, Auditory midbrain and nerve responses to sinusoidal variations in interaural correlation. *J. Neurosci.* **26**, 279–289 (2006). doi:10.1523/jneurosci.2285-05.2006.

- [44] PX Joris, Neural binaural sensitivity at high sound speeds: Single cell responses in cat midbrain to fast-changing interaural time differences of broadband sounds. *The J. Acoust. Soc. Am.* **145**, EL45–EL51 (2019). doi:10.1121/1.5087524.
- [45] I Siveke, SD Ewert, B Grothe, L Wiegreb, Psychophysical and physiological evidence for fast binaural processing. *J. Neurosci.* **28**, 2043–2052 (2008). doi:10.1523/jneurosci.4488-07.2008.
- [46] J Encke, M Dietz, Model code (2021). doi:10.5281/zenodo.5643429.
- [47] A Khintchine, Korrelationstheorie der stationären stochastischen prozesse. *Math. Annalen* **109**, 604–615 (1934). doi:10.1007/bf01449156.
- [48] A Darling, *Properties and implementation of the gammatone filter: a tutorial*. (Speech Hearing and Language, Work in Progress, University College London, Department of Phonetics and Linguistics), pp. 43–61 (1991).
- [49] Q McNemar, *Psychological Statistics*. (John Wiley and Sons inc.), 4th edition, pp. 137–139 (1966).
- [50] H Lüddermann, H Riedel, B Kollmeier, Electrophysiological and psychophysical asymmetries in sensitivity to interaural correlation steps. *Hear. Res.* **256**, 39–57 (2009). doi:10.1016/j.heares.2009.06.010.